THE ROYAL
SOCIETY

Mixing in the shear superposition micromixer: three-dimensional analysis

By Frederic Bottausci, Igor Mezić, Carl D. Meinhart and
Caroline Cardonne

*Department of Mechanical and Environmental Engineering,
University of California, Santa Barbara, CA 93106, USA*
(mezic@engineering.ucsb.edu)

In this paper, we analyse mixing in an active chaotic advection micromixer. The micromixer consists of a main rectangular channel and three cross-stream secondary channels that provide ability for time-dependent actuation of the flow stream in the direction orthogonal to the main stream. Three-dimensional motion in the mixer is studied. Numerical simulations and modelling of the flow are pursued in order to understand the experiments. It is shown that for some values of parameters a simple model can be derived that clearly represents the flow nature. Particle image velocimetry measurements of the flow are compared with numerical simulations and the analytical model. A measure for mixing, the mixing variance coefficient (MVC), is analysed. It is shown that mixing is substantially improved with multiple side channels with oscillatory flows, whose frequencies are increasing downstream. The optimization of MVC results for single side-channel mixing is presented. It is shown that dependence of MVC on frequency is not monotone, and a local minimum is found. Residence time distributions derived from the analytical model are analysed. It is shown that, while the average Lagrangian velocity profile is flattened over the steady flow, Taylor-dispersion effects are still present for the current micromixer configuration.

Keywords: micromixer; lab on a chip; quasi-periodic flow

1. Introduction

The use of integrated microelectromechanical systems (MEMS) is expanding rapidly due to improvements in microfabrication technology. MEMS have applications in a variety of industries, including the automotive, aerospace, computer and biomedical industries. Micro total-analysis systems (μTAS) are being developed for drug discovery, drug delivery and chemical sensing (Chiem *et al*. 1997). Technical barriers of these systems include device packaging and interfacing, chemical surface absorption and control of fluid motion on the microscale (Karniadakis & Beskok 2001). The performance of these devices can be limited by the rate at which mixing occurs at the microscale. Mixing of two fluids can be enhanced when the interface between

the fluids is increased through stretching and folding (Ottino 1989), so that diffusion between the fluids only has to occur over a relatively small distance. At the macroscale, stretching and folding of interfaces is performed by three-dimensional (3D) turbulent eddies that contain a continuous spectrum of length-scales. A turbulent flow regime in channels occurs at a relatively high Reynolds number, defined as $Re = UL/\nu$, where U is the characteristic velocity, L is the characteristic length-scale (e.g. the width of the channel) and ν is the kinematic viscosity. A water flow through a 200 μm wide channel, with a kinematic viscosity $\nu = 10^{-6}$ m^2 s^{-1}, and a characteristic velocity of 1 cm s^{-1} has a Reynolds number of 2. The flow at this Reynolds number is 'strongly' laminar. In microdevices, fluids are often mixed through pure molecular diffusion. However, depending upon the rate at which diffusion occurs, the diffusion time-scale t_D, defined as $t_D = L^2/D$, where L is the relevant mixing length (i.e. the characteristic width of the flow channel), and D is the molecular diffusivity, may be too large. As an example, in practical BioMEMS applications (e.g. biosensors (Vijayendran *et al.* 2003)) one is often interested in transporting and mixing biological molecules. The diffusion coefficient of haemoglobin in water is $D = 70$ μm^2 s^{-1}, and therefore it would take up to 570 s for this molecule to diffuse over a length of $L = 200$ μm. Thus, advective stretching and folding of interfaces is still desirable in order to improve the effective diffusion coefficients. Microscale mixers that were designed to achieve such an improvement can be divided into two broad classifications: passive and active. Passive mixers rely on geometrical properties of channel shape to induce complicated fluid-particle trajectories and thus mix. Examples include work by Branebjerg *et al.* (1994, 1996), Miyake *et al.* (1993), Liu *et al.* (2000), Yi & Bau (2000) and Stroock *et al.* (2002).

Recent passive designs in, for example, Liu *et al.* (2000) and Stroock *et al.* (2002) use the concept of chaotic advection: if the distance between two nearby particles increases, on average, exponentially as they advect through a bounded flow, the particles are said to have chaotic trajectories (Aref 1984; Ottino 1989). These passive designs are such that the flow in the channel is fully 3D, which is a necessary condition for a laminar, steady flow to have chaotic trajectories. The key advantage of chaotic advection-based strategies is that an exponential rate of mixing is achieved as opposed to an algebraic rate (e.g. t^{-1}) that is achieved, for example, by inducing vortical motion (see Ottino (1989) and, for an example in micromixing, Chou *et al.* (2001)).

In contrast, even the first active micromixer, designed by Evans *et al.* (1997), was based on the concept of chaotic advection. Even an essentially two-dimensional (2D) laminar flow can mix well if it is time-periodic (steady 2D flows can only mix at an algebraic, not exponential, rate). The design studied in this paper, which we call the *shear superposition micromixer* (SSM), was first presented in Volpert *et al.* (1999), based on the prior theoretical study of optimal mixing by sequences of shear flows at different angles in D'Alessandro *et al.* (1999). In contrast to Evans *et al.* (1997), this is a continuous through-flow micromixer consisting of the main channel with three cross-flow side channels that are capable of producing time-dependent shear flow in the direction transverse to the main stream (see figure 1). This design was also considered in Lee *et al.* (2001), where a single side-channel configuration was presented. In Niu & Lee (2003) a study of that design with periodic repetition of spatial cells was performed using ideas from chaotic dynamics. In that study the frequency used for actuation of every side channel was the same. It was argued in
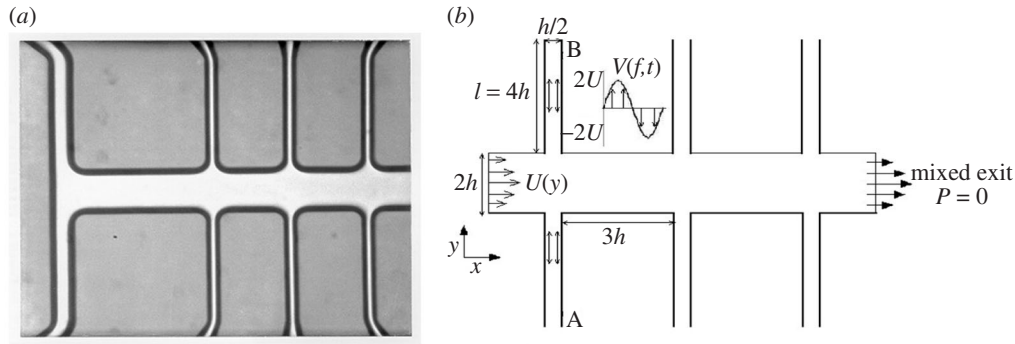
(a) (b)

Figure 1. (a) Micrograph of the working portion of the mixing microchip. (b) Schematic of the fluid flow in the channel. A and B are actively controlled pumps setting V and f: $h = 100 \, \mu\text{m}$; $V(f, t) = 2U \sin(2\pi f t)$.

Volpert *et al.* (1999) that the frequencies of the actuation for downstream channels should increase, not stay the same. This is based on the physical fact that the first side channel introduces layering of two fluid streams. Thus, the size of maximal blobs of non-mixed fluid decreases downstream, and the frequency necessary for good mixing increases. The physical mechanism of mixing in SSM is similar to that described mathematically in D'Alessandro *et al.* (1999) and consists of rearrangement of streamwise-oriented strips to cross-stream oriented strips and subsequent stretching by parabolic shear (somewhat similar to the tendril-whorl map introduced by Khakhar *et al.* (see Ottino 1989), as described in Müller *et al.* (2004). In the same paper, optimization of frequencies for mixing was performed on a 2D model.

The 2D model introduced in Volpert *et al.* (1999) and used in Niu & Lee (2003) is kinematic and consists of a superposition of a parabolic flow profile in the main channel with the solution of the Navier–Stokes equation with oscillatory pressure gradients in the side channels. Here we extend such modelling to the 3D geometry. We also provide a numerical solution to the Navier–Stokes equations and compare it with the kinematic model. Particle image velocimetry (PIV) is performed in the microchannel and compared with numerical simulations and the analytical model.

Evaluating the performance of a chaotic advection micromixer is not a trivial task given that the key part of the process is the layering of fluid interfaces by the flow, in which diffusion plays a negligible role. For the purpose of evaluating that part of the process we use a new measure for mixing called the *mixing variance coefficient* (MVC). The MVC is sensitive both to the advective part of the mixing process, represented by the layering of interfaces, and to the different *scales* on which mixing is taking place. We evaluate the performance of micromixers from experimental data and numerical simulations using MVC.

Understanding Taylor-dispersion properties of a flow in microchannels is an important part of evaluating micromixer performance. We analyse residence time distributions in SSM using the kinematic model.

This paper is organized as follows. We present the micromixer design in § 2. We discuss the model for the flow in § 3, and compare it with numerical simulations and PIV experiments. We discuss the measure of mixing that we use, MVC, in § 4, and show its experimental and numerical evaluations. In § 5 we discuss average Lagrangian veloc-
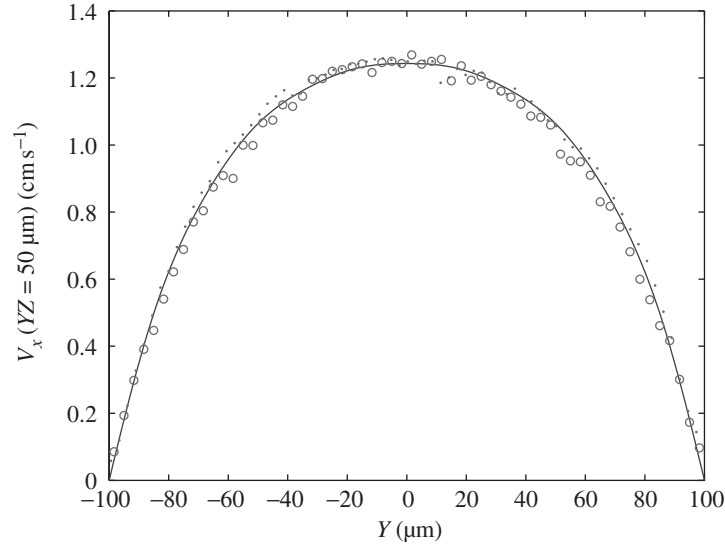
Figure 2. Comparison of analytical expression (solid line), numerical solution (open circles) and experimental PIV measurement (dots) for the steady flow in the main channel. The measurements are performed on a plane indicated at the top channel schematic.

ities (or, equivalently, residence time distributions) in the micromixer. We conclude in §6. In the appendices we provide some details on the solution of Navier–Stokes equations with oscillating pressure gradients, and details of the experimental and numerical techniques used.

2. Micromixer design

The active mixing device consists of a main mixing channel and three pairs of secondary channels that perturb the flow in the main channel. Two unmixed, miscible fluids enter the main channel and are then manipulated by pressure-driven flow from the secondary channels. The flow into the secondary channels oscillates at specified frequencies, providing an enhanced mixing efficiency. As shown in figure 1, the mixing channel is $2h$ high and $13.5h$ long, where h is an adjustable length-scale ranging from 50 to 150 µm, depending on the application of the mixer. In the current paper we keep $h = 100$ µm. The six secondary channels (or three pairs of secondary channels) are perpendicular to the main channel and are $h/2$ wide, $5h$ long and separated from each other by a distance of $3h$. An approximately parabolic profile develops at the entrance of the main channel. In the side channels an oscillatory flow is induced by pumping. The channels are set to oscillate at phases $(0, \pi, 0)$, while the amplitude and frequencies are varied to achieve optimal mixing. This gives a versatile design that can mix efficiently under varying flow conditions.

3. Modelling and numerical analysis

We first discuss a simple model of the flow that consists of a superposition of a steady channel flow in the main channel and unsteady channel flows in the secondary channels. The parameters that we examine here were suggested by a number of
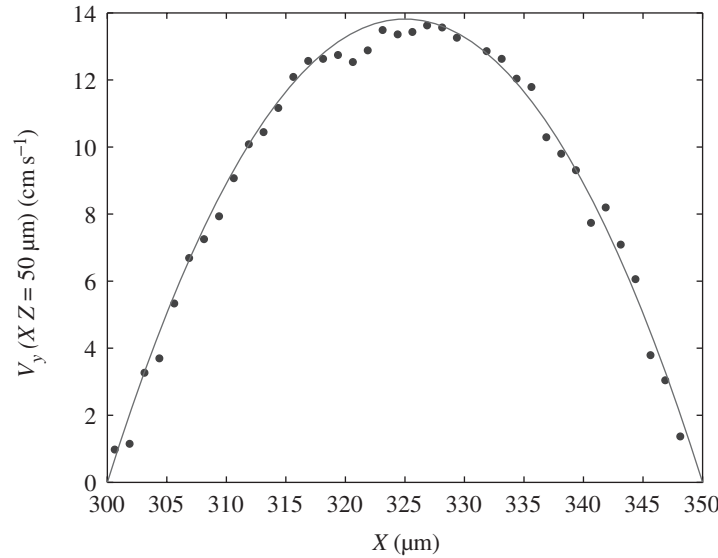
Figure 3. Comparison of velocity in the side channel obtained from numerical simulation (solid line) and an analytical model (closed circles). Maximal velocity for a frequency of 55 Hz.
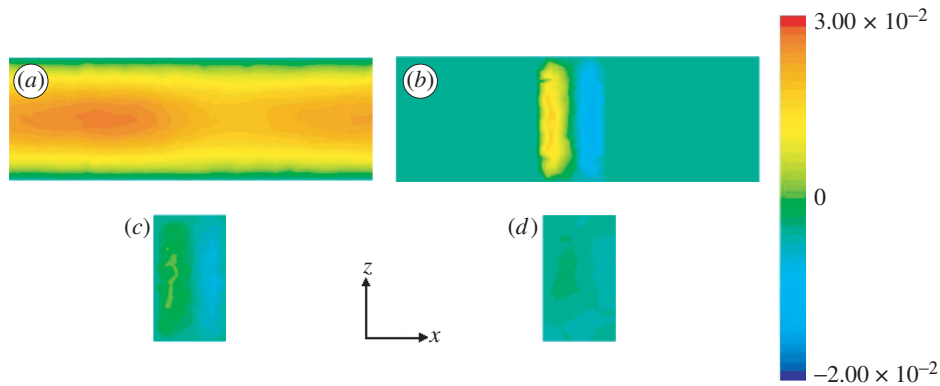

Figure 4. Axial (v_x) velocity for various planes in the micromixer. Axial velocity in (*a*) the $y = 100$ μm plane; (*b*) the $y = 200$ μm plane; (*c*) the $y = 210$ μm plane; and (*d*) the $y = 220$ μm plane.

previous studies (Volpert *et al.* 1999; Müller *et al.* 2004), where optimal frequencies for mixing were studied. The 3D nature of the present investigation shows that the optimal frequencies for mixing are shifted somewhat, but not by a large amount (see § 4).

For the main channel, the solution reads (White 1974)

$$v_x(y, z) = -\frac{16a^2}{\mu\pi^3}\frac{\mathrm{d}p}{\mathrm{d}x}\sum_{i=1,3,5,\ldots}^{\infty}(-1)^{(i-1)/2}\left[1 - \frac{\cosh(i\pi z/2a)}{\cosh(i\pi b/2a)}\right]\frac{\cos(i\pi y/2a)}{i^3}. \quad (3.1)$$

A comparison between numerical simulations using the Fluent package, the exact solution above and experimental (PIV) measurements in the main channel is shown

in figure 2. The details of the PIV measurement are presented in Appendix B. The flow rate in the experiment was $0.9 \, \text{ml} \, \text{h}^{-1}$.

The time-dependent velocity profile in the secondary channels can be determined by solving the Navier–Stokes equations using a Fourier series expansion. In this derivation the flow is assumed to have an oscillatory pressure gradient. We give this derivation in some detail in Appendix A. Note that due to high-frequency oscillations in the side channel, the usual quasi-steady approximation cannot be employed, and the inertial term (local velocity acceleration) has to be kept. The channel is assumed to have a square cross-section with y in the interval $[0, a]$ and z in the interval $[0, b]$ (for convenience we again denote the axial direction in the side channel with x and cross-sectional directions by $\{y, z\}$). For a unidirectional flow $v_x = v(y, z, t)$, subject to a time-periodic pressure gradient

$$\frac{\partial p}{\partial x} = -\rho A \sin(\omega t + \phi), \tag{3.2}$$

where A is a constant. The non-dimensional velocity after transients is given by

$$\left. \begin{aligned} V &= \sum_{m,n \in \mathbb{Z}^+ \text{ odd.}} \frac{16}{\beta m n \pi^2} \frac{1}{1 + (k(m,n)/\beta)^2} \\ &\quad \times \left(\frac{k(m,n)}{\beta} \sin(\tau + \phi) - \cos(\tau + \phi) \right) \sin n\pi\gamma \sin m\pi\eta, \\ k(m,n) &= \left(r(n\pi)^2 + \frac{1}{r}(m\pi)^2 \right), \end{aligned} \right\} \tag{3.3}$$

where $\tau = \omega t$, $\gamma = y/a$, $\eta = z/b$, $r = b/a$ and $\beta = ab\omega/\nu$. Note that for the case considered in the current paper, $b = a/2$. The dimensional velocity v can be obtained from $V = \nu v / Aab$.

Both the Fourier expansions for the steady and the unsteady flows converge fast and are thus easy to evaluate.

In figure 3, we show a comparison between numerical solutions for 28 and 55 Hz (obtained using flat oscillating velocity profiles at the side channel ends) and a velocity obtained from equation (3.3) with the constant A obtained from pressure in numerical simulations. Profiles are shown at the time when velocity in the centre of the side channel is maximal.

Details of the numerical simulation using the commercial software Fluent are provided in Appendix C.

The model formed by superposing velocity (3.1) in the main channel (axial velocity being zero elsewhere) and (3.3) in the side channels (y component of velocity being zero elsewhere) fits the real velocity profile well for a range of parameters for which the nonlinear terms in Navier–Stokes equations can be neglected. For small Reynolds numbers, this is always the case far away from the channel-intersection regions. However, within the channel-intersection regions there are parameter values when nonlinear advective effects are still present. In figure 4, contour plots of numerically evaluated axial velocity in the micromixer are shown. The planes shown are $\{x, z\}$ at different y positions, with the oscillation frequency set at 28 Hz. A simple order-of-magnitude estimate of terms in Navier–Stokes equations shows that, despite a low Reynolds number, the nonlinear terms for parameters used in this simulation cannot
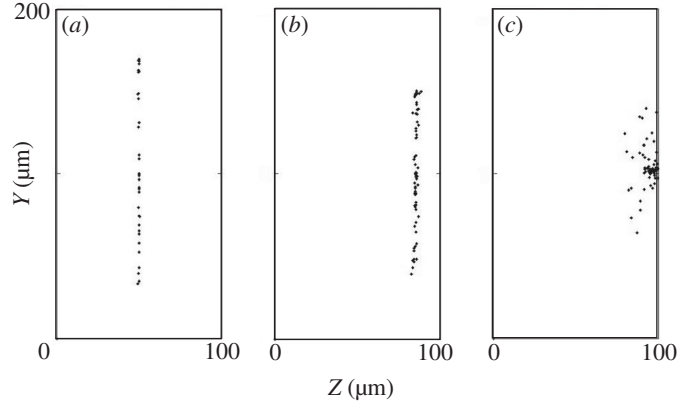
Figure 5. Projection onto the $\{y, z\}$-plane ($x = 0$) of the main channel of a set of particles starting at different times. (a) Starting in the centre of the entrance plane ($z = 0.5h$). (b) Starting at $y = h$, $z = 0.9h$ in the entrance plane. (c) Starting at $y = h$, $z = 0.95h$ in the entrance plane.

be neglected in the zone that lies in the intersection of side channels and the main channel. This is indicated by the deficit in the axial velocity seen in figure 4a, for plane $y = 100\,\mu$m. Figure 4b shows non-zero axial velocity in the intersection region, at plane $y = 200\,\mu$m. This velocity, which is due to nonlinear terms, decays inside the side channel, as shown in figure 4c, d. Axial velocity in the side channels decays to zero at *ca.* 20 μm into the secondary channel. Beyond that, the solution in the secondary channel is given by (3.3).

4. Mixing variance coefficient measurements

We are interested in the distribution of fluid particles starting at the entrance plane $x = 0$. Particle paths mostly reside in a 2D plane $z = \mathrm{const.}$ at the same height that the main channel's particles started from. This is illustrated in figure 5, where it is clear that weak departure from planar motion occurs only close to the wall of the channel.

Formally, particle paths are governed to a first approximation by a velocity field of the form

$$\left.\begin{aligned}
\dot{x} = v_x(x, y, z, t) = \frac{\partial \psi(x, y, z, t)}{\partial y}, \\
\dot{y} = v_y(x, y, z, t) = -\frac{\partial \psi(x, y, z, t)}{\partial x}, \\
\dot{z} = 0.
\end{aligned}\right\} \tag{4.1}$$

Such is the form of the analytical model described in the previous section. A flow of this form cannot be mixing in the dynamical systems sense. However, the specific purpose of the device is to mix fluid entering from one side of the main channel ($x = 0$, $y \leqslant 100$) with fluid entering from the other side of the main channel ($x = 0$, $y > 100$). By mixing at each plane $z = \mathrm{const.}$, a flow of form (4.1) could mix this specific initial distribution. To measure the extent to which this happens, we introduced the so-called MVC (Volpert *et al.* 1999). Rigorous definition and mathematical analysis of properties of pseudo-norms such as MVC can be found in Mathew *et al.* (2003a). In the current 3D analysis MVC is defined as follows.
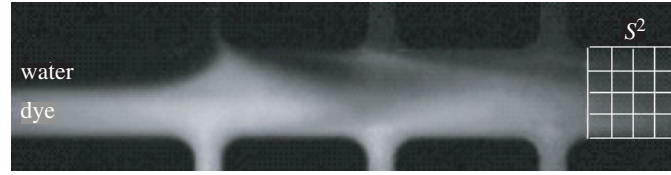
Figure 6. Photograph with indication of the $\{x, y\}$-domain in which the MVC measurement is taken. The frequency of side-channel oscillation is 28 Hz.
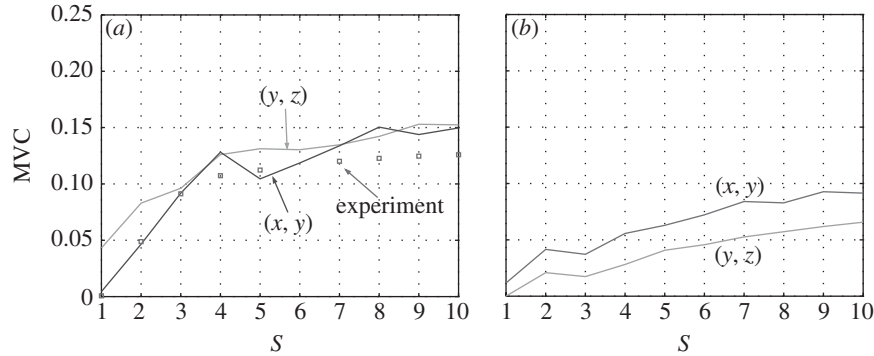

Figure 7. (*a*) Experimental measurement of MVC for an $\{x, y\}$-plane, numerical simulation for an $\{x, y\}$-plane (squares), and numerical simulation for a $\{y, z\}$-plane for a single side channel operating. (*b*) Numerical simulation of MVC for an $\{x, y\}$-plane and a $\{y, z\}$-plane.

  (i) Label particles entering the main channel ($x = 0$, $y > 100$) by one and those entering at $x = 0$, $y \leqslant 100$ by zero.

 (ii) Take an arbitrary intersection of a plane and the microchannel (one example being $x = 1200\,\mu\mathrm{m}$).

(iii) Split the resulting plane into S^2 boxes, and compute the following quantity:

$$\mathrm{MVC}(s) = \frac{1}{S^2} \sum_{i=1}^{S^2} (\rho_i - 0.5)^2,$$

where ρ_i is the average of particle labels (zero or one) over the ith box.

Clearly, the minimum of MVC is zero, while the maximum is 0.25. The minimum occurs when in every box there is an equal number of particles with label one and zero. The maximum occurs when in every box there are either particles with label one or particles with label zero. Note that MVC is invariant with respect to relabelling of particles ($1 \rightarrow 0$, $0 \rightarrow 1$). This definition of MVC is easily extended to experimentally measured concentration fields, as shown in figure 6. The interrogation region is split into sub-boxes and indicated at the exit of the side channel region in figure 6.

The results from measurements and numerical simulations are shown in figure 7*a*. On the horizontal axis, the value labelled S is the square root of the number of boxes used to evaluate MVC. Part (*a*) is with one side channel operating at 28 Hz. It can be seen that the quality of mixing decreases substantially with scale.
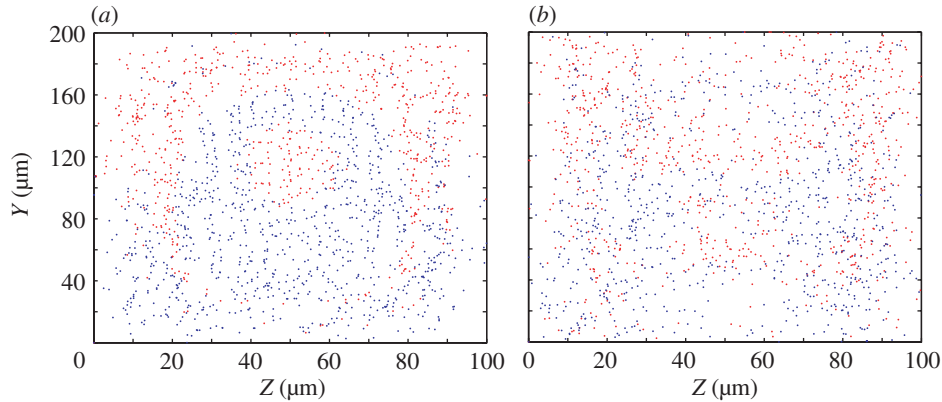
Figure 8. Distribution of fluid particles at the exit of the channel with (*a*) the first
side channel activated; and (*b*) all three side channels activated.

The experimental measurements and numerical-simulation results are quantitatively close, even for numerical simulations in the $\{x, z\}$-plane, for which experimental results are not available. This indicates a degree of isotropy of mixing. Note also that experimental results show somewhat better MVC at smaller scales. This might be due to a smoothing effect of the finite-time resolution. In figure 7*b* results are shown of the numerical simulation with three side channels operating at increasing frequencies of oscillation: 26.025 Hz for the first, 59.34 Hz for the second and 92.925 Hz for the last side channel. The MVC values at smaller scales are substantially improved compared with the case when only a single side channel is oscillating. This shows that mixing improves when two or more downstream side channels are employed and when frequencies of oscillation are increasing for downstream side channels.

Some particle distributions from which MVC was computed are shown in figure 8 for the frequencies indicated above. It can be seen that with only one side channel activated a large unmixed area close to the walls remains. With three side channels activated that area is gone.

It is interesting to inquire about an optimal frequency for mixing. MVC allows for this. In figure 9 we present MVC for actuation of a single side channel. Frequencies that provide good mixing are in the range 40–60 Hz for the range of frequencies and amplitudes studied. In figure 10 we show MVC with single-channel optimal frequency (taken here to be 55 Hz), three side channels operating at the same frequency (55 Hz) and three side channels operating at frequencies of 55, 110 and 220 Hz. It is seen that even at optimal single-channel frequency, mixing is substantially improved by adding two channels oscillating at higher-frequency values. It is possible that a single channel at high frequency mixes even better than the single channel with 55 Hz frequency shown here (i.e. we found a local minimum of MVC), provided the amplitude of oscillation is changed. However, employing all three side channels for mixing adds substantial robustness to the mixing protocol.

In figure 11 we show particle distributions for two different exit planes for the set of frequencies 55, 110 and 220 Hz. Visually, the quality of mixing is good and confirms quantitative results presented in figure 10.
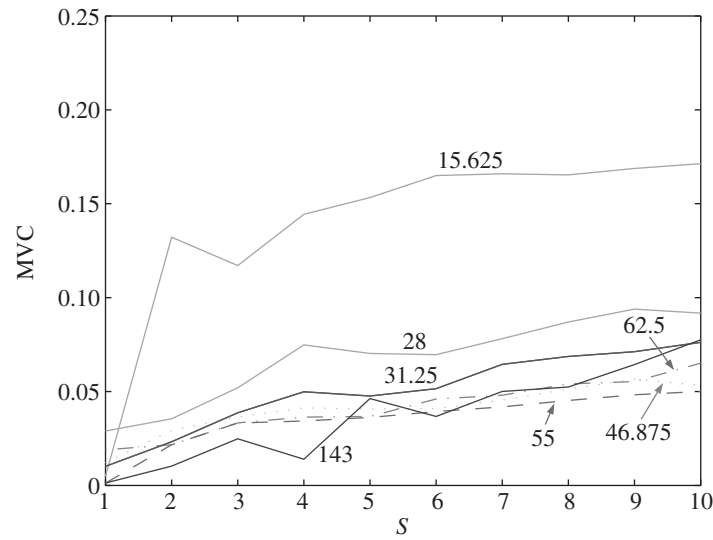
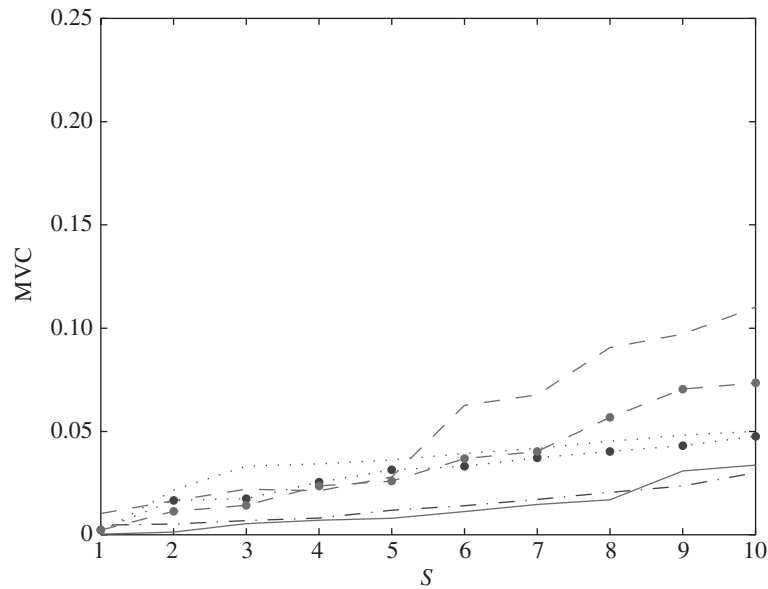Figure 9. MVC for various frequencies when a single side channel is oscillating.

Figure 10. MVC computed from the numerical simulation. The MVC is computed at the channel exit for x between 1200 and 1350 μm for the $\{x, y\}$-plane: dotted line, MVC for one secondary channel activated at 55 Hz; dotted line interspersed with solid circles, MVC for three secondary channels activated at 55 Hz; and dot–dashed line, MVC for three secondary channels activated at 55, 110 and 220 Hz. The MVC is computed at the channel exit for $x = 1350$ μm for the $\{y, z\}$-plane: dashed line, MVC for one secondary channel activated at 55 Hz; dashed line interspersed with solid circles, MVC for three secondary channels activated at 55 Hz; and solid line, MVC for three secondary channels activated at 55, 110 and 220 Hz.

5. Residence times

An important part of the analysis of transport in microchannels is the evaluation of residence times. In biomedical applications Taylor dispersion is often an unwanted feature and thus it is desirable that residence times are as uniform as possible. In accord with Mezić *et al.* (1999), plotting average axial Lagrangian velocities is (for finite channel) equivalent to plotting residence time plots. However, the average Lagrangian velocity plots have the advantage of asymptotically resembling Poincaré maps (Mezić *et al.* 1999) for steady spatially periodic or time-periodic flows. In the present study, where the time-dependence of the flow is quasi-periodic, average axial velocity plots turn out to be quite useful for dispersion analysis. As a test, we computed average axial velocity when no side channels were oscillating and recovered the steady velocity profile given in equation (3.1), as shown in figure 12*a*. Figure 12*b* shows average velocities after a single oscillating side channel. Figure 12*c* shows average velocities after three oscillating side channels when particles are released at time zero. Figure 12*d* shows average velocities after three oscillating side channels when particles are released at one-quarter of the period of oscillation of the first channel. It can be seen that the average velocities with three oscillating side channels have a plateau and thus the flow is 'flatter' than the steady flow. However, peak average Lagrangian velocities are comparable with the peak velocity in the steady flow: substantial Taylor dispersion remains. This is to be expected due to the predominantly 2D nature of the flow. Despite the ability of the flow to mix the particular initial distribution well, fluid particles in this flow do not sample the entire cross-section of the channel, and thus Taylor dispersion is present (Mezić *et al.* 1996).

6. Conclusions

In this paper we analysed some of the properties of mass transport in the SSM. A 3D analytical model was derived by superposing a steady, constant-pressure-gradient solution for the main channel and an oscillatory pressure-gradient solution for the three side channels. Three-dimensional numerical simulation of the Navier–Stokes equation was performed and analysed. This is found to be well approximated by the analytical solution away from the intersection of the channels region. PIV measurements in the microchannel were performed and compared with the numerical and analytical results. Mass transfer in the micromixer is mostly advective on the length-scales and time-scales considered. We pursued analysis of mixing using the MVC, a measure for mixing that differentiates properties of mixing at various spatial scales. Measurements of MVC with a single side channel oscillating were performed and compared with numerical computations. We showed that MVC is substantially improved by using out-of-phase oscillations of all three side channels, as compared with the single side-channel oscillation. Use of more than three channels leads to diminishing returns for improvement of mixing. Indeed, work on 2D models indicates that improvement is largest when going from one to two side channels (Mathew *et al.* 2003*b*). An optimization of mixing by single side-channel oscillation at a fixed amplitude using MVC as the cost function showed that the optimal frequency of oscillation for the current geometry and flow conditions was *ca.* 50 Hz for the range of frequencies studied. Another important tool for understanding mass transfer in channels is the residence time, or equivalently average axial Lagrangian velocity. We
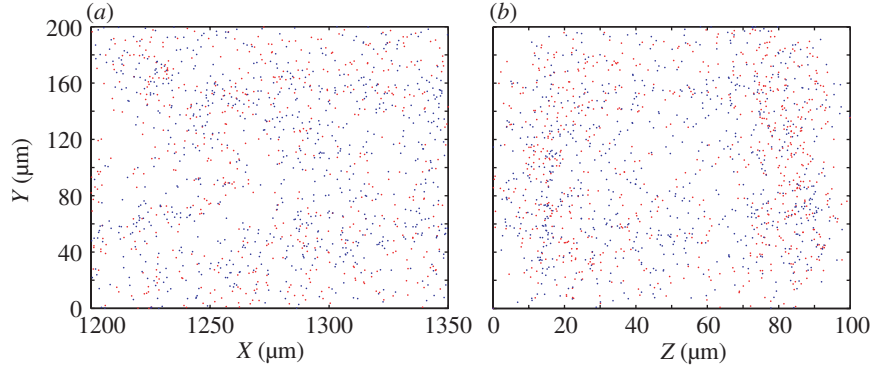
Figure 11. (*a*) Particle distribution at the channel exit in the $\{x, y\}$-plane.
(*b*) Particle distribution at the channel exit in the $\{y, z\}$-plane.

studied these and concluded that, while the profile of average Lagrangian veloci-
ties is substantially flatter than the profile of steady axial velocity, effects of Taylor
dispersion are still present at this length-scale and number of side channels.

Appendix A.

The time-dependent velocity profile in the secondary channels can be determined by
solving the Navier–Stokes equations using a Fourier series expansion. The channel
is assumed to have a square cross-section with y in the interval $[0, a]$ and z in the
interval $[0, b]$. The coordinate x now represents the direction along the axis of the side
channel. For a unidirectional flow $v_x = v(y, z, t)$, subject to a time-periodic pressure
gradient, the dimensional equations become

$$\frac{\partial v}{\partial t} - \nu \left(\frac{\partial^2 v}{\partial y^2} + \frac{\partial^2 v}{\partial z^2} \right) = -\frac{1}{\rho} \frac{\partial p}{\partial x},$$

$$\frac{\partial p}{\partial x} = -\rho A \sin(\omega t + \phi).$$

Thus

$$\frac{\partial v}{\partial t} - \nu \left(\frac{\partial^2 v}{\partial y^2} + \frac{\partial^2 v}{\partial z^2} \right) = A \sin(\omega t + \phi),$$

with the no-slip boundary conditions

$$v(0, z, t) = v(a, z, t) = v(y, 0, t) = v(y, b, t) = 0, \tag{A 1}$$

and the initial condition

$$v(y, z, 0) = v_0(y, z). \tag{A 2}$$

We introduce non-dimensional variables $(\tau = \omega t, \gamma = y/a, \eta = z/b, V = \nu v/Aab)$.
The non-dimensional equation reads

$$\frac{ab\omega}{\nu} \frac{\partial V}{\partial \tau} - \frac{b}{a} \left(\frac{\partial^2 V}{\partial \gamma^2} \right) - \frac{a}{b} \left(\frac{\partial^2 V}{\partial \eta^2} \right) = \sin(\tau + \phi).$$
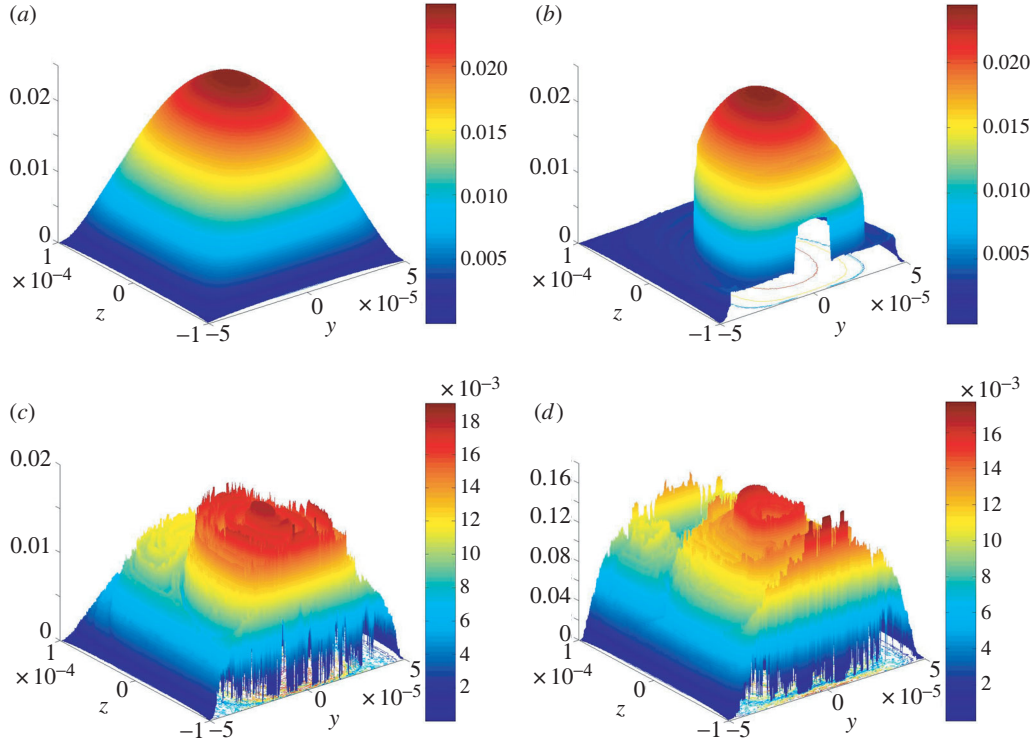
Figure 12. Average Lagrangian velocities in the micromixer with frequencies of oscillation 55, 110 and 220 Hz for the first, second and third side channel, respectively. (*a*) Average Lagrangian velocities with no side channels oscillating, yielding steady velocity profile. (*b*) Average Lagrangian velocities with the first side channel oscillating. (*c*) Average Lagrangian velocities with three side channels oscillating at frequencies of 50, 110 and 220 Hz. Particles released at $x = 0$ plane at time zero. (*d*) Average Lagrangian velocities with three side channels oscillating at frequencies of 50, 110 and 220 Hz. Particles released at $x = 0$ plane at one-quarter of the period of oscillation of the first side channel.

We let $r = b/a$, $\beta = ab\omega/\nu$ and obtain

$$\beta\frac{\partial V}{\partial \tau} - r\left(\frac{\partial^2 V}{\partial \gamma^2}\right) - \frac{1}{r}\left(\frac{\partial^2 V}{\partial \eta^2}\right) = \sin(\tau + \phi). \tag{A 3}$$

The boundary conditions are

$$v(0, \eta, \tau) = v(1, \eta, \tau) = v(\gamma, 0, \tau) = v(\gamma, 1, \tau) = 0. \tag{A 4}$$

We are going to seek the solution using the variation-of-constants method. For this purpose we first solve the homogeneous equation

$$\beta\frac{\partial V}{\partial \tau} - r\left(\frac{\partial^2 V}{\partial \gamma^2}\right) - \frac{1}{r}\left(\frac{\partial^2 V}{\partial \eta^2}\right) = 0. \tag{A 5}$$

Note that any function of the form

$$f(t)\sin n\pi\gamma \sin m\pi\eta, \quad m, n \in \mathbb{Z}^+/\{0\}, \tag{A 6}$$

satisfies the boundary conditions (A 4). Plugging (A 6) into (A 5) and denoting by a dot the time derivative with respect to τ, we get

$$\beta \dot{f} \sin n\pi\gamma \sin m\pi\eta + \left(r(n\pi)^2 + \frac{1}{r}(m\pi)^2 \right) f \sin n\pi\gamma \sin m\pi\eta = 0,$$

thus implying

$$\dot{f} + \frac{1}{\beta} \left(r(n\pi)^2 + \frac{1}{r}(m\pi)^2 \right) f = 0$$

with solution

$$f(\tau) = f_0^{m,n} \exp\left(-\frac{1}{\beta} \left(r(n\pi)^2 + \frac{1}{r}(m\pi)^2 \right) \tau \right).$$

Thus, the homogeneous solution to A 3 is

$$V = \sum_{m,n=1}^{\infty} f_0^{m,n} \exp\left(-\frac{1}{\beta} \left(r(n\pi)^2 + \frac{1}{r}(m\pi)^2 \right) \tau \right) \sin n\pi\gamma \sin m\pi\eta.$$

The idea of the variation-of-constants method is to assume a solution for (A 3) to be

$$V = \sum_{m,n=1}^{\infty} f_0^{m,n}(\tau) \exp\left(-\frac{1}{\beta} \left(r(n\pi)^2 + \frac{1}{r}(m\pi)^2 \right) \tau \right) \sin n\pi\gamma \sin m\pi\eta.$$

Plugging this into (A 3) and setting

$$k(m,n) = \left(r(n\pi)^2 + \frac{1}{r}(m\pi)^2 \right),$$

we obtain

$$\sum_{m,n=1}^{\infty} \beta \dot{f}_0^{m,n} \exp\left(-\frac{k(m,n)}{\beta}\tau \right) \sin n\pi\gamma \sin m\pi\eta$$

$$- \sum_{m,n=1}^{\infty} f_0^{m,n} k(m,n) \exp\left(-\frac{k(m,n)}{\beta}\tau \right) \sin n\pi\gamma \sin m\pi\eta$$

$$+ \sum_{m,n=1}^{\infty} f_0^{m,n} k(m,n) \exp\left(-\frac{k(m,n)}{\beta}\tau \right) \sin n\pi\gamma \sin m\pi\eta$$

$$= \sin(\tau + \phi) \sum_{m,n=1}^{\infty} a_{m,n} \sin n\pi\gamma \sin m\pi\eta,$$

where

$$a_{m,n} = \frac{\int_0^1 \int_0^1 \sin n\pi\gamma \sin m\pi\eta \, d\gamma}{\int_0^1 \int_0^1 \sin^2 n\pi\gamma \sin^2 m\pi\eta \, d\gamma} \, d\eta$$

$$= \begin{cases} \dfrac{16}{mn\pi^2}, & \text{for } m, n \text{ odd,} \\ 0, & \text{otherwise.} \end{cases}$$

The numbers $a_{m,n}$ are coefficients of the expansion of the unit constant function into basis functions $\sin n\pi\gamma \sin m\pi\eta$. Thus, we get

$$\dot{f}_0^{m,n} = \frac{a_{m,n}}{\beta} \sin(\tau + \phi) \exp\left(\frac{k(m,n)}{\beta}\tau\right). \tag{A 7}$$

To simplify, we assume $\phi = 0$. Solving (A 7) gives

$$f_0^{m,n} = \begin{cases} c_{m,n} + \dfrac{16}{\beta mn\pi^2}\left(\dfrac{\mathrm{e}^{(k(m,n)/\beta\tau)}}{1+(k(m,n)/\beta)^2}\left(\dfrac{k(m,n)}{\beta}\sin\tau - \cos\tau\right)\right. \\ \qquad\qquad\qquad\qquad\left. + \dfrac{1}{1+(k(m,n)/\beta)^2}\right), \quad m,n \text{ odd,} \\ \\ c_{m,n}, \qquad\qquad\qquad\qquad\qquad\qquad\qquad\qquad\quad \text{otherwise,} \end{cases}$$

so the solution is given by

$$V = \sum_{m,n=1,2}^{\infty} c_{m,n} \exp\left(-\frac{k(m,n)}{\beta}\tau\right) \sin n\pi\gamma \sin m\pi\eta$$

$$+ \sum_{m,n \text{ odd.}} \frac{16}{\beta mn\pi^2}\left(\frac{1}{1+(k(m,n)/\beta)^2}\left(\frac{k(m,n)}{\beta}\sin\tau - \cos\tau\right)\right.$$

$$\left. + \frac{\exp(-k(m,n)/\beta\tau)}{1+(k(m,n)/\beta)^2}\right) \sin n\pi\gamma \sin m\pi\eta,$$

where $c_{m,n}$ are determined from initial conditions.

Appendix B. PIV measurements

The principle of the micro-PIV measurements is to take two successive snapshots of the flow, previously filled with particles small enough to follow the flow. Each image is split into cells. The spatial correlation of the cells gives the displacement of the particles in each cell. The vector velocity associated with the cell is then calculated knowing the time step between two images. The PIV gives the velocity field in the considered plane. The micro-PIV measurements, an extension of the work in Santiago *et al.* (1998) and Meinhart *et al.* (1999, 2000), are performed using a YAG Laser ($\lambda = 532$ nm). The pulses are carried through a fibre-optic cable to the illumination port of a Nikon Eclipse TE 200 inverted microscope. The light then passes through a long-pass filter cube (epi-fluorescent prism) and a numerical aperture (NA) = 0.75 $40\times$ Nikon objective lens. Fluorescent-dyed 691 nm diameter flow-tracing polystyrene particles absorb in green wavelength ($\lambda = 532$ nm) and emit in red ($\lambda = 575$ nm). On the way back, the light passes through the objective lens and the filter cube before reaching the 1030 bits $\times$ 1300 bits $\times$ 12 bits interline CCD cooled camera. The filter cube filters out green light from background reflection to let the red light pass. The camera feature allows back-to-back recording of two images within a minimum time of 500 ns. The laser-pulse duration combined with the decay time of the fluorescent dye is *ca.* 5–10 ns, which enables us to have a picture of the flow with a freezed motion. In the experiment the delay time between two images is set to 1.8 µs. The images captured by the CCD camera are analysed with PIV software developed

by Steve Wereley (Department of Mechanical Engineering, Purdue University, IN). The interrogation windows (cells) are 256 pixels × 64 pixels with an overlap of 50% giving a resolution of 20.22 µm × 5.05 µm. The out-of-plane measurement depth is *ca.* 2 µm. Twelve image pairs are cross correlated and the correlation functions are then averaged before the peak detection in order to increase the accuracy of the measurements (Meinhart *et al.* 2000). The velocity profiles are measured in the secondary channels (50 µm × 100 µm) at the abscissa $z = 50$ µm for a frequency of 55 Hz, when the velocity is maximum. Images are taken 200 µm from the main channel to eliminate the entrance effects. The velocity profile results from averaging eight velocity measurements.

(*a*) *Images with fluorescent dye*

The two fluids to be mixed are injected into the main channel using a programmable syringe pump PHD 2000 and two 10 ml syringes filled with dye in one and degassed deionized water in the other. Each transverse channel is connected through hard tubing to a microsyringe (0.5 µl). The syringe plug is attached to a motor (solenoid). A function generator drives the motor at the desired frequency generating the pull–push effect on the fluid in the transverse channels. The image analysis is performed using a Nikon Eclipse E 600FN microscope. The source light is a 100 W mercury lamp connected directly to the illumination port of the microscope. The white light thus generated is reflected by an epi-fluorescent filter cube Nikon B-2A and relayed to an NA 0.3 10× objective lens. The fluorescent dye used is acridine orange (diluted at 33% in degassed deionized water). It absorbs the blue (490 nm) light and emits green (530 nm) light. The fluorescent light imaged by the objective lens passes through the filter cube, where blue light from the background reflections is filtered out. The remaining green light is focused onto a 1280 bits × 1024 bits × 12 bits CCD camera. The exposure time of the camera is proportional to the image brightness and therefore cannot be smaller than 2.02 ms. This exposure time does not freeze the main flow which moves *ca.* 25 µm. The image recorded is normalized between zero and one, split into S^2 cells and then the MVC is computed. The density ρ_i (MVC equation) is associated with the ith box according to the average pixels' intensity over that box (intensity = 0 for a black pixel).

Appendix C.

We performed numerical simulations using the finite-volume commercial software Fluent that solves Navier–Stokes equations using a second-order implicit unsteady scheme. It ran in parallel on eight processors with an average clock time of 2.5 s per iteration. The meshing was automatically performed using the software Gambit providing a micromixer volume split into 366 139 tetrahedral cells. The working fluid was water at 20 °C. In order to reach a residual smaller than 10^{-8}, 130 iterations were performed at each time step. The fluid was injected at the two entrances of the main channel with a flat velocity profile. The flow rate in the main channel was constant and equal to 0.9 ml s^{-1} (0.45 ml s^{-1} for each entrance). At the extremities of the secondary channels the velocity was imposed to be flat with time dependence $(U_i = \hat{U}_i \sin(2\pi f_i t + \Phi_i), i = 1, 2, 3)$. The control parameters are the frequencies f_i, the phase shift Φ_i and the amplitude of oscillations imposed by the value of $\hat{U}_i$. To

visualize and characterize the mixing of two fluids, particles were injected at the two entrances of the main channel.

References

Aref, H. 1984 Stirring by chaotic advection. *J. Fluid Mech.* **143**, 1–21.

Branebjerg, J., Fabius, B. & Gravesen, P. 1994 Application of miniature analysers from microfluidic components to µTAS. In *Proc. Micro Total Analysis System Conf., Twente, Netherlands*, pp. 141–151.

Branebjerg, J., Fabius, B. & Gravesen, P. 1996 Fast mixing by lamination. In *Proc. 9th Annual Workshop on Microelectromechanical Systems, San Diego, CA*, pp. 441–446.

Chiem, N., Colyer, C. & Harrison, D. J. 1997 Microfluidic systems for clinical diagnostics. In *Int. Conf. on Solid State Sensors and Actuators, Chicago, IL*, vol. 1, pp. 183–186.

Chou, H.-P., Unger, M. A. & Quake, S. R. 2001 A microfabricated rotary pump. *Biomed. Microdevices* **3**, 323–330.

D'Alessandro, D., Dahleh, M. & Mezić, I. 1999 Control of mixing in fluid flow: a maximum entropy approach. *IEEE Trans. Automatic Control* **44**, 1852–1863.

Evans, J., Liepmann, D. & Pisano, A. P. 1997 Planar laminar mixer. In *Proc. 10th Annual Workshop Microelectromechanical Systems, Nagoya, Japan*, pp. 96–101.

Karniadakis, G. E. & Beskok, A. 2001 *Micro flows.* Springer.

Lee, Y. K., Deval, J., Tabeling, P. & Ho, C. M. 2001 Chaotic mixing in electrokinetically and pressure-driven micro flows. In *Proc. 14th IEEE Workshop on MEMS, Interlaken, Switzerland*, pp. 483–486.

Liu, R. H., Sharp, K. V., Olsen, M. G., Stremler, M. A., Santiago, J. G., Adrian, R. J., Aref, H. & Beebe, D. J. 2000 A passive micromixer: three-dimensional serpentine microchannel. *J. MEMS* **9**, 190–197.

Mathew, G., Mezić, I. & Petzold, L. 2003*a* A multiscale measure for mixing and its applications. In *Proc. Conf. on Decision and Control, Maui, HI, USA*.

Mathew, G., Mezić, I., Serban, R. & Petzold, L. 2004 Optimization of mixing in an active micromixing device. In *Technical Proc. 2004 NSTI Nanotechnology Conf. Trade Show, Boston, MA*, vol. 1, pp. 300–303. Cambridge, MA: Nano Science and Technology Institute.

Meinhart, C. D., Wereley, S. T. & Santiago, J. G. 1999 Measurements of a microchannel flow. *Exp. Fluids* **27**, 414–419.

Meinhart, C. D., Wereley, S. T. & Santiago, J. G. 2000 A PIV algorithm for estimating time-averaged velocity fields. *J. Fluids Engng* **122**, 285–289.

Mezić, I., Brady, J. F. & Wiggins, S. 1996 Maximal effective diffusivity for time periodic incompressible fluid flows. *SIAM J. Appl. Math.* **56**, 40–57.

Mezić, I., Wiggins, S. & Betz, D. 1999 A method for visualization of invariant sets of dynamical systems based on the ergodic partition. *Chaos* **9**, 173–182.

Miyake, R., Lammerink, T. S. J., Elwenspoek, N. & Fluitman, J. H. J. 1993 Micromixer with fast diffusion. In *Proc. IEEE Microelectromechanical Workshop, Fort Lauderdale, FL*, pp. 248–253.

Müller, S. D., Mezić, I., Walther, J. H. & Koumoutsakos, P. 2004 Transverse momentum micromixer optimization with evolution strategies. *Comput. Fluids* **33**, 521–531.

Niu, X. & Lee, Y. K. 2003 Efficient spatiotemporal chaotic mixing in microchannels. *J. Micromech. Microengng* **13**, 454–462.

Ottino, J. M. 1989 *The kinematics of mixing: stretching, chaos and transport.* Cambridge University Press.

Santiago, J. G., Wereley, S., Meinhart, C. D., Beebe, D. J. & Adrian, R. J. 1998 A PIV system for microfluidics. *Exp. Fluids* **25**, 316–319.

Stroock, A. D., Dertinger, S. K. W., Ajdari, A., Mezić, I., Stone, H. A. & Whitesides, G. M. 2002 Chaotic mixer for microchannels. *Science* **295**, 647–651.

Vijayendran, R. A., Motsegood, K. M., Beebe, D. J. & Leckband, D. E. 2003 Evaluation of a three-dimensional micromixer in a surface-based biosensor. *Langmuir* **19**, 1824–1828.

Volpert, M., Mezić, I., Meinhart, C. D. & Dahleh, M. 1999 An actively controlled micromixer. In *Proc. ASME Mechanical Engineering International Congress and Exposition, MEMS, Nashville, TN*, pp. 483–487.

White, F. M. 1974 *Viscous fluid flow.* McGraw-Hill.

Yi, M. & Bau, H. H. 2000 The kinematics of bend-induced stirring in micro-conduits. In *Proc. MEMS 2000*, vol. 2, pp. 489-496. New York: ASME.